Heliyon 9 (2023) e20707

Contents lists available at ScienceDirect

Heliyon

journal homepage: www.cell.com/heliyon

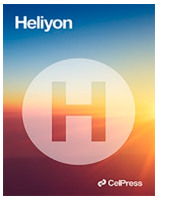

Biosynthesis of silver nanoparticles using tea leaf extract (*camellia sinensis*) for photocatalyst and antibacterial effect

Khoi Tran Khac [a,b], Hiep Hoang Phu [a], Hue Tran Thi [a], Van Dinh Thuy [a], Hue Do Thi [a,*]

[a] *Thai Nguyen University of Education, No. 20, Luong Ngoc Quyen Street, Quang Trung Ward, Thai Nguyen City, 25000, Viet Nam*
[b] *Faculty of Fundamental Science, Phenikaa University, Nguyen Van Trac Street, Yen Nghia Ward, Ha Dong District, Hanoi City, Ha Dong, 100000, Viet Nam*

ARTICLE INFO

Keywords:
C.AgNPs
Camellia Sinensis
Photocatalyst
Antibacterial

ABSTRACT

Silver nanoparticles (C. AgNPs) are synthesized by the biological reduction method using extracts from green tea leaves (*Camellia Sinensis*) collected from tea hills at an altitude of 100 m above the ground. The chemicals present in the tea leaf extract act as reducing agents used to reduce Ag^{+} ions to silver atoms to form C. AgNPs in the solution. In this work, we optimized the C. AgNPs synthesis process by investigating the influence of reaction parameters such as concentration of tea leaf extract (1 ppm–50 ppm), reaction temperature (30 °C-60 °C), reaction time (5 min–100 min), and reaction rate (400 rpm–800 rpm) through absorption UV–Vis spectroscopy, TEM transmission electron microscopy, and spectroscopy X-ray. Organic compounds in tea leaf extract are detected by NMR measurement. The functional groups on the C. AgNPs are shown on the Fourier transform infrared (FTIR) spectrum. The C. AgNPs are used to degrade MB dye at 10 ppm concentration based on the photocatalytic effect using a 6500 K white light source. The C. AgNPs have also been studied for their antibacterial activity on two bacteria, *Pseudomonas aeruginosa* (P. A) and *Staphylococcus aureus* (S.A), while a positive control is *Ampicillin* 50 mg/ml and a negative control is H_2O. The results reveal that the C. AgNPs with diameters in the range of 25 nm–55 nm degrade 10 ppm MB dye after 1 h with photodegradation efficiency up to 96 %. The antibacterial ability of C. AgNPs against both bacteria is good, even superior to that of *Ampicillin*. Furthermore, the particle synthesis efficiency and therefore the antibacterial activity as well as the photodegradation effect of C. AgNPs are higher than previously reported. At the same time, using green tea leaf extract to synthesize C. AgNPs creates environmentally friendly products. These useful behaviors are the potential to increase the scope and applicability of C. AgNPs, especially for biomedical applications in the near future.

1. Introduction

Nanotechnology is an area of research and innovation concerned with the development of atomic and molecular-based materials and devices. Today the development and advancements of nanotechnology have brought new solutions to the problems that hinder the development of poor countries, especially in relation to health and hygiene, food security, and the environment. Nanotechnology offers

* Corresponding author.
E-mail address: huedt@tnue.edu.vn (H. Do Thi).

https://doi.org/10.1016/j.heliyon.2023.e20707
Received 30 May 2023; Received in revised form 30 August 2023; Accepted 4 October 2023
Available online 5 October 2023

cheaper and more reliable drug delivery systems that can provide cleaner energy sources [1–3]. At the same time, nanomaterials with biological activities can become filters to purify the environment [4,5].

Along with the development of each country, water contaminants are extremely abundant in that the water is contaminated with organic and inorganic dyes which are products of the garment, food, cosmetic, and paper industry, etc [6,7]. These substances do not decompose by themselves but accumulate, causing water pollution and environmental pollution, negatively impacting human life for a very long time if not handled promptly. Therefore, treating and cleaning dyeing wastewater is a very necessary job for humans, aiming for a pollution-free environment and improving the quality of human life.

There are many methods for the treatment of dyeing wastewater, each of which has its strengths and weaknesses [8–10]. In recent years, the use of nanoparticles to treat dyeing wastewater is receiving the most attention from scientists because of their small size, large surface area, ability to absorb light in the visible region high ant, and faster equilibrium rate [11–15]. Among them, AgNPs with outstanding physical, chemical, and biological features have shown their ability in dyeing wastewater treatment through a photocatalytic effect [16–19]. Various methods have used AgNPs to treat dyeing wastewater in photocatalytic applications. AgNPs can be used to create the potential for metal-based catalysts and other materials to be applied to degrade organic pollutants or treat wastewater as an efficient technology under UV radiation [19–21]. AgNPs impregnated with metal oxides such as TiO_2, and ZnO significantly increase the photocatalytic efficiency of these metal oxides [22]. In addition, the Chitosan/Ag complex, or the presence of Ag on the glass or wood substrates also provides photocatalytic effects with high efficiency [20,23–25]. These methods AgNPs or Ag oxide act as catalysts to increase the photodegradation efficiency. Although the degradation time is faster, these methods require more complex synthesis techniques and colorant degradation is limited by the formation of multiple catalyst layers [26]. AgNPs synthesized using plant extracts are also used directly to degrade organic dyes. For example, AgNPs synthesized from *Parkia speciosa* leaf extract degrade MB in 3 h to about 84% [22]. AgNPs synthesized from *Saccharomyces cerevisiae* leaf extract degrade MB in 6 h–85% [23]. Through consulting many documents related to this issue, we found that the synthesis of AgNPs using plant extracts has not really been controlled. The resulting AgNPs come in a variety of shapes and sizes, leading to their limited use in applications. For example, in photocatalyst applications, it has been reported that the photodegradation efficiency is less than 90%. Our research aims to improve the synthesis efficiency and increase the applicability of AgNPs. The photocatalytic mechanism of AgNPs has been explained in Ref. [27] and is briefly mentioned as follows: when excited by light AgNPs release Ag ions and free electrons, forming electron-hole pair. The dye molecules are decomposed by an oxidation reaction with the holes. At the same time, the presence of reducing agents such as H_2O_2 or $NaBH_4$ forms $OH^{\cdot}$ which can degrade the dye by reduction reaction.

In addition, AgNPs are also used in many other outstanding applications such as being used as substrates for surface-enhanced Raman scattering (SERs), detection of organic dyes [18,27,28], transmission, delivery of drugs and biomolecules [29–31], and antibacterial and kill bacteria, kill viruses [32–34]. Although the antibacterial mechanism of AgNPs is controversial, some of the main mechanisms can be mentioned as follows: (i) AgNPs can release Ag ions which can penetrate the cell wall and cytoplasmic membranes disrupt bacterial envelopes, inactivate respiratory enzymes, disrupt cell membranes, and transform deoxyribonucleic acid (DNA) [35]. (ii) Silver ions can inhibit protein synthesis by denaturing ribosomes in the cytoplasm. (iii) In addition to the ability to release silver ions, AgNPs can kill bacteria on their own by accumulating in pits formed on the cell wall causing denaturation of the cell membrane [36]. AgNPs are also able to penetrate the bacterial cell wall and alter the structure of the cell membrane [36].

In this study, we optimized the factors participating in the reaction such as extract concentration, temperature, time, and reaction rate to synthesize C. AgNPs with the best efficiency. The C. AgNPs were used to study the photocatalytic activity applied to the degradation of MB dye under the excitation of 6500 K white light. Experiments were designed in the presence or absence of C. AgNPs to see the role of C. AgNPs in increasing the degradation efficiency of MB dye. At the same time, C. AgNPs were studied for their antibacterial activity against P.A and S.A strains with the positive control being *Ampicillin* antibiotic and the negative control being H_2O.

2. Materials and methods

2.1. Materials

Silver nitrate ($AgNO_3$, >99%) and methylene blue dye ($C_{16}H_{18}ClN_3S$, 97%), Sodium borohydride ($NaBH_4$, >99%) and Hydrogen peroxide solution (H_2O_2, 30% (w/w) in H_2O) were purchased from Sigma Aldrich and Merck (Germany), respectively. The deionized water (DI) with a resistance of 18.2 MΩ was used in all processes. The chemicals were used without any further cleaning. Green tea leaves are not too old and not too young picked from a hill about 100 m above the ground in the mountains in the Northern part of Vietnam.

2.2. Camellia Sinensis leaf extract preparation

The green tea leaves are washed with water several times and finally rinsed with distilled deionized water to remove impurities. The leaves were chopped, air-dried, and then dried in an oven at 50 °C for about 24 h. The dried leaves are then pulverized with a blender and further smoothed with an agate mortar. Twenty grams of tea leaf powder is put into a 100 ml water tank. The mixture was autoclaved at 100 °C for 10 min, then centrifuged at 3000 rpm to collect the solution. The resulting solution was filtered through Whatman paper No 1, then through a Ministart filter 0.22 μm in pore diameter. The *Camellia Sinensis* leaf extract was stored at 4 °C and used for about 1 month.

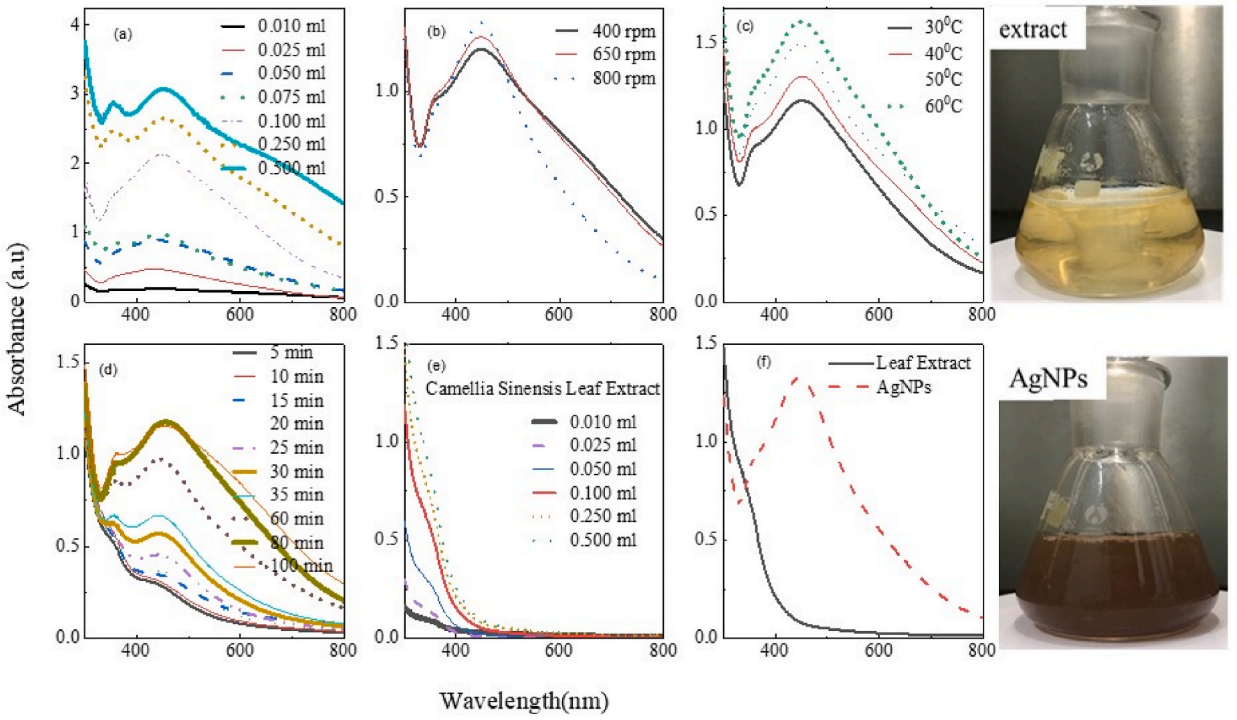

Fig. 1. Absorbance spectrum of AgNP solutions when changing extract volume (a), magnetic stirring speed (b), reaction temperature (c), and reaction time (d). The absorption spectrum of tea leaf extract with different extract volumes (e) and the absorption spectrum of tea leaf extract and silver nanoparticle solution with the same extract concentration (f). The two inserted images show the colors of tea leaf extract and AgNPs solution. (For interpretation of the references to color in this figure legend, the reader is referred to the Web version of this article.)

2.3. Green synthesis of silver nanoparticles from Camellia Sinensis leaf extract (C.AgNPs)

Firstly, 6 ml of 10 mM $AgNO_3$ solution was slowly added to a volume of the prepared *Camellia Sinensis* leaf extract, under magnetic stirring conditions for about 2 h at a temperature varying between 30 °C and 60 °C. Second, after the ending of the reactions, the resulting solution is yellow-brown. The solution was centrifuged three times and re-dispersed in water with the same volume for further studies. To investigate the influence of the factors participating in the reaction on the formation of C. AgNPs, we designed independent experiments in which the speed of magnetic stirring, reaction temperature, and concentration of extract were respectively changed. To know the optimal time for a particle fusion reaction, a certain amount of sample was drawn to investigate the UV–Vis spectrum at different times.

2.4. C.AgNPs in photocatalysis application

The MB degradation efficiency was evaluated through the absorption spectrum of MB over time of irradiation in the presence of C. AgNPs catalyst. A 30 W LED lamp which has a 6500 K color temperature (Philips, Amsterdam, The Netherlands) was used as the visible light source. The mixture of 100 ml of 10 ppm MB and 60 ml of purified C. AgNPs was stirred at 800 rpm for 2 h in the dark. Add 0.5 ml of H_2O_2 10% or 0.5 ml of $NaBH_4$ 0.2 M to the solution as catalysts for photodegradation reactions. Then, the mixture was illuminated by an LED light source and the absorption spectrum was investigated after certain irradiation periods to determine the photo-degradation efficiency of MB.

2.5. C.AgNPs in antibacterial applications

Pseudomonas aeruginosa (PA - ATCC 9027), also known as blue pus, is a common bacterium that causes disease in animals and humans. Staphylococcus aureus (AS - ATCC 25923) is a gram (+) bacteria. It is part of the dermal resident microbiome found in both the nose and skin. SA can cause many different infections. All bacteria are pre-cultured in Luria bertani (LB) medium overnight in a shaker at 37 °C. Using a cork borer drill 5 wells 0.6 cm in diameter on the dish and add 100 μL of the mixture of materials. The plates are incubated at 37 °C for 18 h after being refrigerated for 1 h. C. AgNPs particles are diluted in 1 ml of water to obtain different concentrations: 50 μl C. AgNPs solution/1 ml H_2O (5×10^{10} particles/ml), 25 μl C. AgNPs solution/1 ml H_2O (2.5×10^{10} particles/ml), 12.5 μl C. AgNPs solution/1 ml H_2O (1.25×10^{10} particles/ml). The antibacterial activity assay was performed according to the method in Refs. [37–39]. Deionized water was used as the negative control and the antibiotic *Ampicillin* 50 μg/ml was used as the

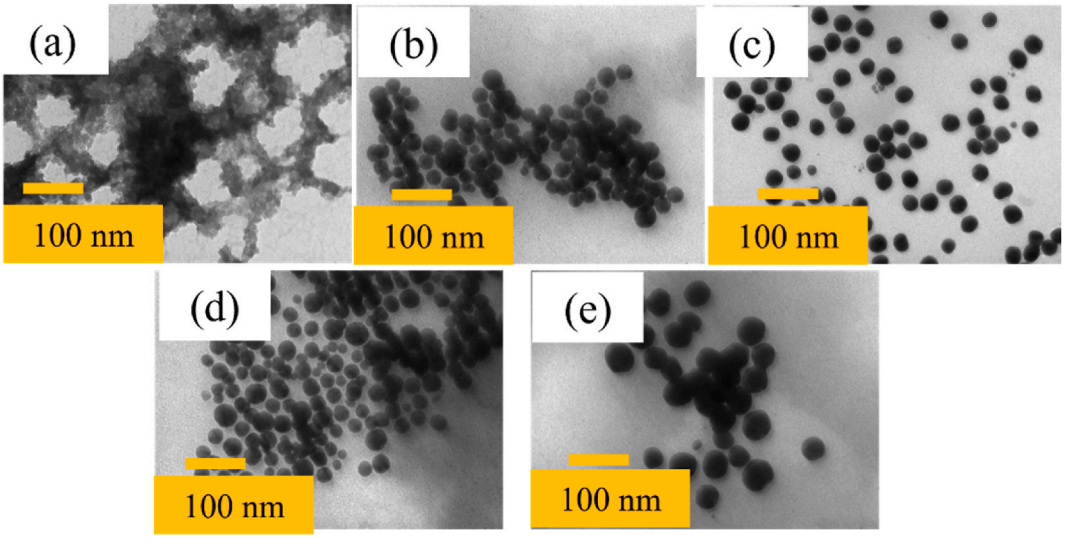

Fig. 2. TEM images of C. AgNPs with different extraction volumes: 0.025 ml (a), 0.075 ml (b), 0.1 ml (c), 0.25 ml (d) and 0.5 ml (e).

positive control. The antibacterial activity of C. AgNPs was assessed through the diameter of the zone of inhibition.

3. Materials characterization

UV–Vis absorption spectrum working on the system Jasco V-770 UV–Vis spectrophotometer in the range of 250 nm–1000 nm allows for investigation of the optical properties of C. AgNPs and their photocatalytic ability. The morphology and size of C. AgNPs were investigated by using a JEOL JEM-1010 transmission electron microscope (TEM) operating at 80 kV. The structure and physical properties of the C. AgNPs were studied by the XRD spectra using an X-ray diffractometer (Bruker D8 Advance, Germany). The functional groups on C. AgNPs were determined by Fourier transform infrared (FTIR) Spectroscopy on the system Cary 600 Series FTIR spectrometer, range 7500–2800 cm^{-1} and the composition of organic compounds in the tea leaf extract was determined using nuclear magnetic resonance (NMR) measurements performed on NMR Bruker Avance III equipped with PABBO BB/19F–1H/D 5 mm with Z gradient, including auto-matching and auto-tuning, 550 Hz frequency, using N_2 as cooling liquid gas.

4. Result and discussions

In this section, we present the results of synthesizing C. AgNPs using green tea leaf extract by investigating the influence of the factors participating in the reaction to optimize the synthesis yield. Also, present the results on the antibacterial and photocatalytic activities of C· AgNPs. The influence of factors in the synthesis of C. AgNPs particles was investigated through the plasmon absorption spectrum of the solutions. The optical properties of silver nanostructures depend on their shape and size. The plasmon absorption peak of silver nanostructures can range from near ultraviolet to near-infrared depending on their structure. The spherical AgNPs in water have UV–Vis absorption spectra with a characteristic resonance peak in the visible light region from about 400 nm to 600 nm depending on the size. Each size band has a characteristic resonance peak position. The color change of the solution from light yellow (begin) to dark brown (end) marked the formation of C. AgNPs (Fig. 1). The absorption spectra of the solutions were obtained when changing the volume of a tea leaf extract from 0.01 ml (1 ppm) to 0.5 ml (50 ppm) (Fig. 1a), and changing the stirring speed from 400 rpm to 850 rpm (Fig. 1a and b), change of reaction temperature 30 °C, 40 °C, 50 °C, 60 °C (Fig. 1c). The results show that the concentration of the extract greatly affects the formation of C· AgNPs. When the extract volume is less than 0.1 ml (10 ppm), the plasmon resonance peaks are wide and the absorbance is low, indicating that the particles have formed but are not uniform in shape and size, and the synthesis efficiency is not high. When the volume of tea leaf extract was increased, the plasmon resonance spectra had a narrower half-width and higher absorbance. However, when the extraction volume is large at 0.25 ml and 0.5 ml, on the absorption spectrum in addition to the resonance peak at 450 nm, which is typical for spherical C. AgNPs, there is also an additional resonance peak at 350 nm. This peak is attributed to the contribution of the absorption spectrum of the tea leaf extract (Fig. 1f). Because of the absorption spectrum of the tea leaf extract (Fig. 1e and f), it is shown that when the concentration of the extract is high, the absorption margin in the 350 nm region has a high absorbance. At the same time, when the volume of extract in solution is higher than 0.1 ml, the absorption spectra have high absorbance in the 700 nm to near-infrared region. This proves that in the solution appear large C· AgNPs. Using 0.1 ml of tea leaf extract (10 ppm in concentration) for the highest C. AgNPs synthesis yield. Analysis of the absorption spectrum when changing the magnetic stirring speed can confirm that at 800 rpm, the obtained spherical C. AgNPs have the highest uniformity in shape and size (Fig. 1b). Temperature also affects the size and concentration of C· AgNPs. According to our survey, the temperature increased from 30 °C to 60 °C, and C. AgNPs formed more uniformly and were smaller in size. This is reflected in the half-width of the

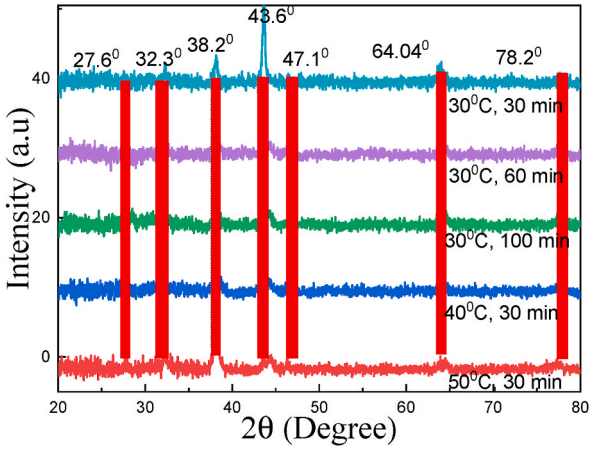

Fig. 3. X-ray spectra of C. AgNPs at different reaction temperatures and times.

narrowing spectra, the resonance peak shifts from 545 nm to 445 nm, and the absorbance increases from 1.15 to 1.6.

Analysis of the absorption spectrum of the sample according to the reaction time shows that the most suitable time to synthesize C. AgNPs is about 80 min because at that time the synthesis efficiency of the particles is the greatest and there are no by-products (Fig. 1d). The results of investigating the morphology and size of C. AgNPs on TEM images are also consistent with the analysis results from the absorption spectrum when changing the volume of tea leaf extract (Fig. 2a – e). When the extract volume was 0.025 ml (2.5 ppm), C. AgNPs were 25 nm in average diameter with low concentration. When the extract volume was 0.075 ml (7.5 ppm), synthesized C. AgNPs were about 35 nm in size, however, the size distribution is wide. With an extracted volume of 0.1 ml (10 ppm), the synthesized C. AgNPs had the highest uniformity in shape and size with an average size of about 40 nm. As the extract volume increased, the size distribution spectrum increased, and the average size of C. AgNPs was about 55 nm. The above results show that the extract concentration, temperature, time, and reaction rate affect the formation and growth of C. AgNPs in the solution. The suitable parameters for the synthesis of C. AgNPs include an initial extract concentration of 10 ppm, stirring speed from 800 rpm, reaction temperature of 60 °C, and reaction time of 80 min.

The crystal structures of C. AgNPs at different reaction temperatures and times are shown on x-ray spectra (Fig. 3). The observed diffraction peaks at positions $2\theta = 27.6^\circ, 32.3^\circ, 38.2^\circ, 43.6^\circ, 47.1^\circ, 64.04^\circ, 78.2^\circ$ corresponding to the lattice planes characteristic of the face-centered cubic structure fcc are: (210), (122), (111), (200), (103), (220), (311) as correlated to JCPDS no 04–0783 and in Ref. [20]. The detection of no other peaks from any other phase evidenced that single-phase Ag with cubic structure nanoparticles has been obtained directly.

NMR spectra of green tea samples with different concentrations in Thai Nguyen in Vietnam showed that the chemical composition of tea samples was similar to the main chemical composition. About 30 compounds have been identified in the 1H NMR spectrum, and more than 50 signals or groups of signals have been shown. In addition to common compounds such as amino acids and fatty acids and common sugars such as sucrose and glucose; Signals of phenols, flavonoids (flavan-3-ols or catechins, flavonols), and xanthines can be observed.

In the region 0–3 ppm of tea leaf extract concentration, significant signals were detected for Theanine, which is found only in tea, quinic acid, and theogallin (Fig. 4a). The small signals in this region are mainly of fatty acids and of α-amino acids. Small signals were recognized as those of sugars in 3–5 ppm concentrations, with sucrose giving the most obvious signal (Fig. 4b). Caffeine is the main xanthine observed in the spectrum with a significant signal. Small differences in the chemical composition of the green tea solution can be observed in different places, especially tea in Bac Kan. The chemical components in tea in Thai Nguyen represent the typical components in tea, so we choose tea here as a raw material for AgNPs synthesis.

Five common catechins (EGCG, EGC, ECG, EC, C) and some unknown catechins (probably (−) - gallocatechin-3-gallate (GCG), (−) - gallocatechin (GC), (−) - catechin-3-gallate (CG), (−)-epigallo-catechin-3-(3″-*O*-methyl) - gallate, (−) - epigallocatechin-3,5-digallate, (−) - epicatechin- 3,5-digallate, or epiafzelechin was detected mainly in the region between 2.3 – 3 ppm and 5–8 ppm [40]. EGC and ECG signals were observed to be insignificant in this region due to the possibility. This family of compounds can be easily identified by the characteristic signals arising from H-3 (3.80–5.20 ppm) and H-4 (2.50–3),10 ppm) of the heterocyclic ring. Small signals in the region of 5–8 ppm are mainly those of kaempferol and quercetin glycosides (flavonols) along with signals of gallic acid, theogallin, and possibly *p*-coumaroyl quinic acid (Fig. 4c).

The FTIR analysis was used to characterize and identify the biomolecules responsible for the C·AgNP's synthesis. The results of infrared spectroscopy of the obtained C. AgNPs are shown in Fig. 5. The band at 3442 cm^{-1} can be assigned to stretching free hydroxyl groups (νO-H) in Catechin, and Gallic acid. The marked peak at 1060 cm^{-1} can also be related to the stretching vibration of the plant extract's C–OH bond from proteins. The peaks at 1384 cm^{-1} arise from the C–N stretching mode of aromatic amine groups in Theanine. The band at 1640 is mainly attributed to the stretching vibrations of the C–N bond of amide functional groups or from the C═O stretching mode in Catechin, Gallic acid, and Theanine. On the other hand, the intense and broad peak at 386 cm^{-1} corresponded to the Ag metal [41,42].

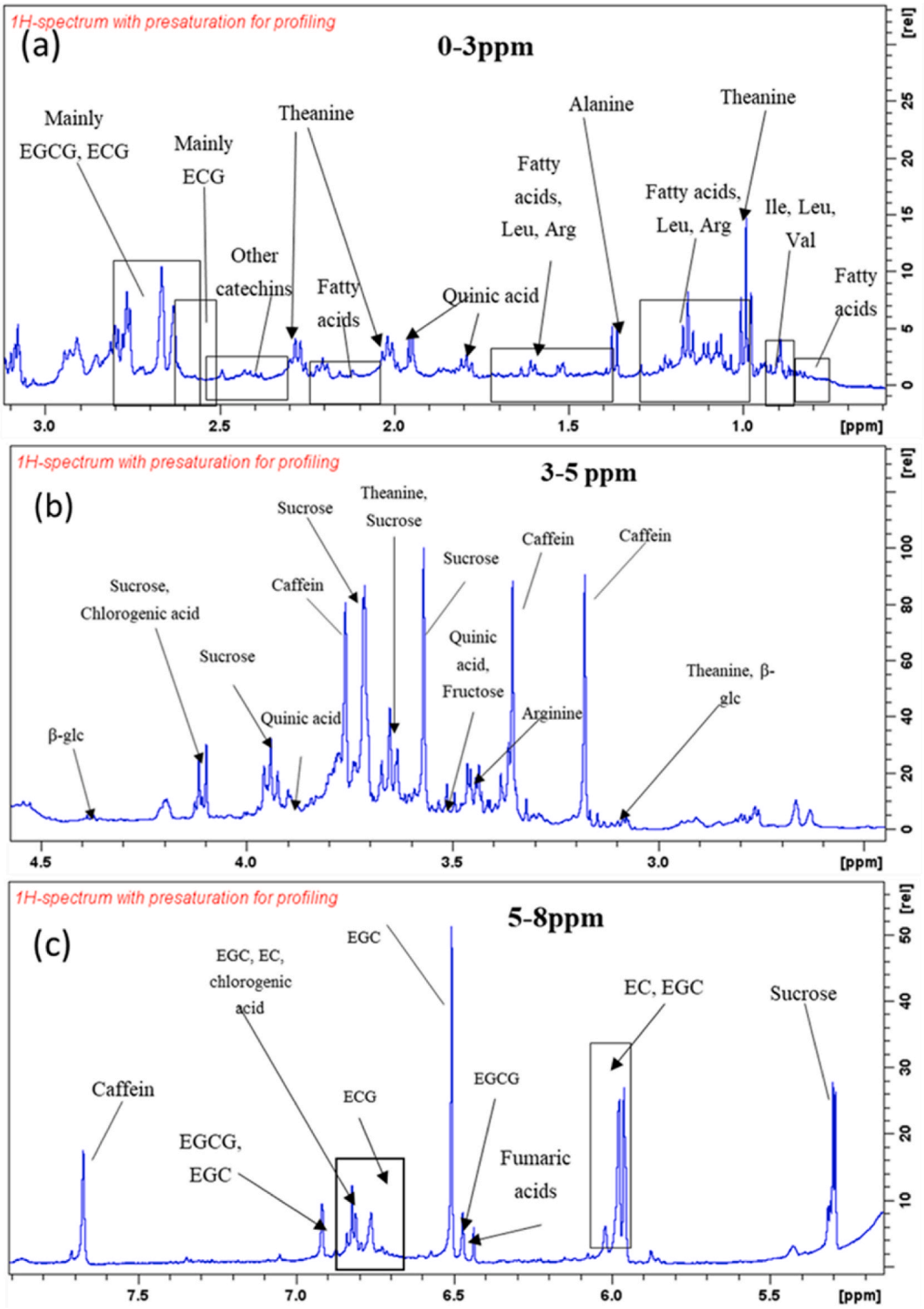

Fig. 4. NMR spectrum of the green tea samples with different concentrations (a) 0–3 ppm, (b) 3–5 ppm, and (c)5–8 ppm. (For interpretation of the references to color in this figure legend, the reader is referred to the Web version of this article.)

Fig. 6 is the absorption spectra investigating the photodegradation of MB dye in the presence of H_2O_2 (Fig. 6a) or $NaBH_4$ only (Fig. 6c) and in the presence of C. AgNPs (Fig. 6b, d). The absorption spectra in Fig*ure 6* only have the characteristic absorption peak at 662 nm of the MB colorant appears, but the resonance peak of the plasmon of C. AgNPs is not observed because the concentration of C.

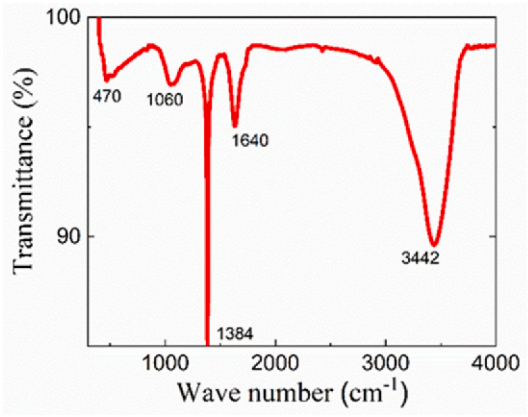

Fig. 5. FTIR spectra of C. AgNPs synthesized from Camellia Sinensis leaf extract.

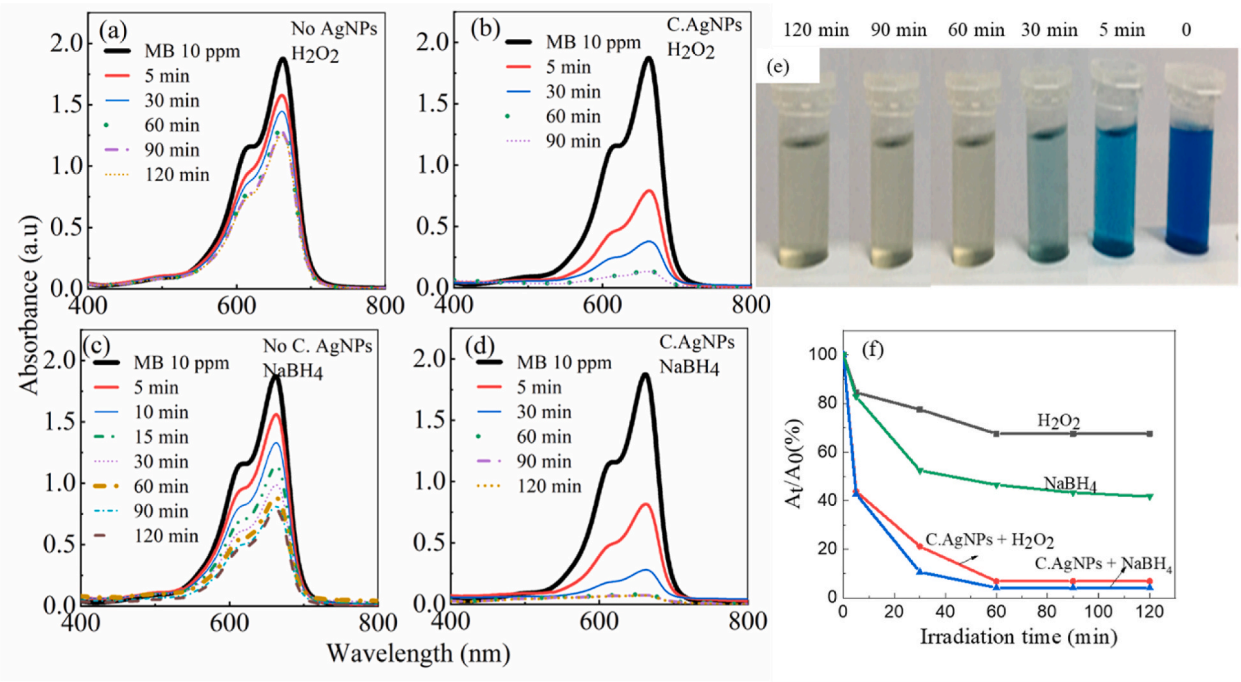

Fig. 6. Absorbance spectra of the original 10 ppm MB and its absorption spectra upon photodegradation over time of irradiation in case (a) no C. AgNPs, H_2O_2, (b) C. AgNPs, H_2O_2, (c) no C. AgNPs, $NaBH_4$, (d) C. AgNPs, $NaBH_4$. (e) The color of MB solutions with decomposition time in the presence of C. AgNPs and H_2O_2, (f) dependence of relative absorbance on irradiation time. (For interpretation of the references to color in this figure legend, the reader is referred to the Web version of this article.)

AgNPs is too low compared to that of the MB concentration. The decline in absorbance of MB dye when illuminated by visible light indicates that the pigment undergoes photodegradation with time. MB with a characteristic absorption peak at 662 nm, the initial absorbance without decomposition was 1.87. The MB degradation efficiency at the concentration of 10 ppm increased more slowly after 120 min of irradiation in the presence of H_2O_2 or $NaBH_4$. MB decomposition performance in the presence of $NaBH_4$ is better than in the presence of H_2O_2. However, the degradation rate of MB dye is not high. When C. AgNPs were added to the solutions and illuminated under the same conditions, a clear change in the degradation rate and photodegradation efficiency was observed (Fig. 6b, d). After 1 h of illumination in the presence of C. AgNPs in the solution, the absorbance of MB dye was significantly reduced. This is demonstrated when comparing the absorption decline of the dye through the A_t/A_0 ratio over time in the solutions (Fig. 6e) and the color change of the pigment solution (Fig. 6f). These results clearly demonstrate the catalytic role of C· AgNPs. The photodegradation efficiency can be determined by the following formula (1):

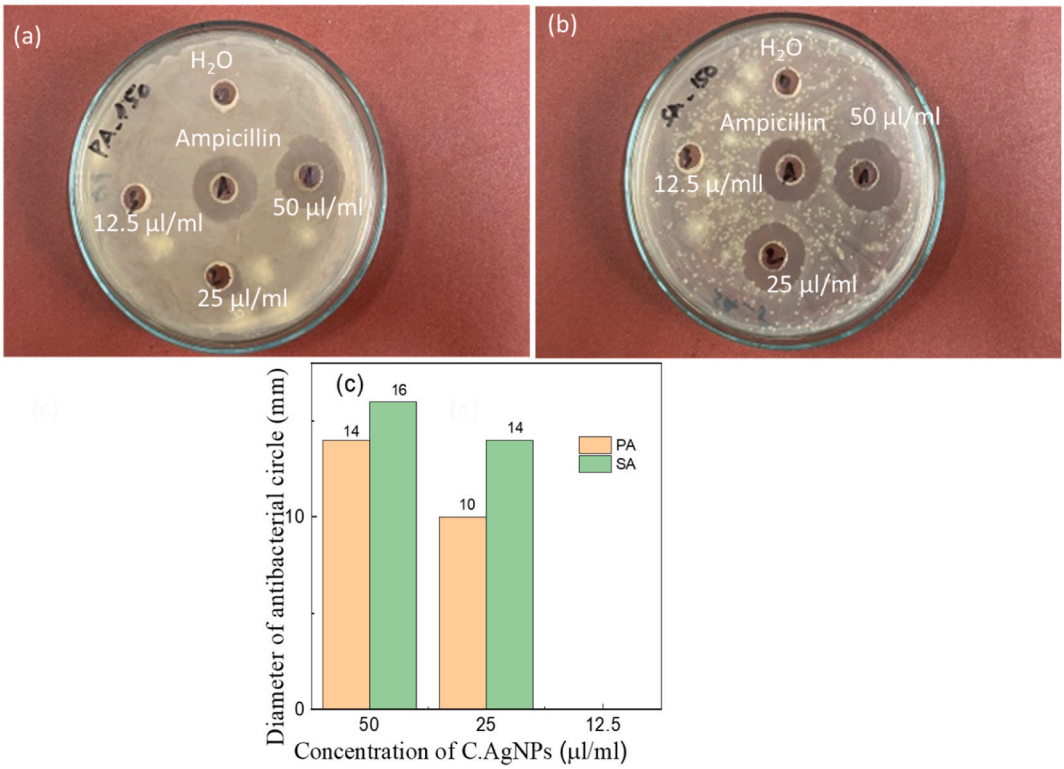

Fig. 7. Image of antibacterial circles when using antibiotics Ampicillin and different concentrations C. AgNPs on bacterial strains P.A (a), bacteria S. A (b) and diagram showing the dependence of ring diameter antibacterial on the concentration of C. AgNPs (c).

$$H = \frac{A_0 - A_t}{A_0} \times 100\ \%. \quad (1)$$

A_0 is the absorbance of initial MB, and A_t is the absorbance of MB at 662 nm when in solution illuminated for time t. From the data on the absorption spectrum, it can be calculated that the optical absorption efficiency of C. AgNPs in the range of 60 min of illumination is 32.5% (only H_2O_2), 53.8% (only $NaBH_4$), 93.1% (H_2O_2 + C. AgNPs) and 96% ($NaBH_4$ + C. AgNPs).

The photodegradation mechanism of MB dye is explained by the series of equations (2)–(6) as below:

$$AgNPs + h\nu \rightarrow Ag^+ (e^-, h^+) \quad (2)$$

$$H_2O_2 + e^- \rightarrow HO^\bullet + OH^- \quad (3)$$

$$Ag^+ + H_2O_2 \rightarrow Ag^{+\bullet}O_2H + H^+ \quad (4)$$

$$Ag^{+\bullet}O_2H + H_2O_2 \rightarrow Ag^+ + O_2 + {}^\bullet OH \quad (5)$$

$$OH^\bullet + MB \rightarrow \text{colorless reduction products} \quad (6)$$

$$h^+ + MB \rightarrow \text{colorless oxidation products} \quad (7)$$

H_2O_2 promotes the generation of many photo radicals. OH, which increases the decomposition rate of MB. Meanwhile, the presence of C. AgNPs in the case of $NaBH_4$ reducing agent reduces the activation energy and thus increases the reaction rate. Comparing the photocatalytic results of AgNPs, our C. AgNPs in this report provide superior degradation performance especially when using $NaBH_4$ reductant [43,44].

Fig. 7 is the antibacterial results of C. AgNPs performed on two bacteria PA and SA. The level of antibacterial activity is expressed through the size of the zone of inhibition (gray circle in Fig. 7a and b). The larger the diameter of the zone of inhibition, the better the antibacterial ability. The antibacterial ability of C. AgNPs was compared with the antibacterial ability of H_2O (negative control) and *Ampicillin* antibiotic (positive control). The results show that the concentration of C. AgNPs greatly affects the antibacterial results. With the concentration of C. AgNPs 5×10^{10} particles/ml, the antibacterial ability of the particles against both bacteria is the best and the sterile circle has a larger diameter than the sterile circle when using *Ampicillin*. The specific numbers are shown in Fig. 7c. The antibacterial effect depends on many factors such as the structure, shape, size, and concentration of AgNPs. Although controversial, the

antibacterial mechanism focuses on two main causes: the release and penetration of silver ions into the cell and the direct impact of AgNPs to disrupt the structure or inhibit cytoplasmic growth processes [45,46].

5. Conclusions

In summary, the spherical C. AgNPs were effectively synthesized by the biological reduction method using reducing agents present in *Camellia Sinensis* leaf extract. The results of surveying the influence of factors involved in particle syntheses such as extract concentration, reaction temperature, speed, and time showed the optimal parameters for the synthesis process with high efficiency in which the concentration of extract 10 ppm, suitable stirring speed 800 rpm, reaction temperature 60 °C and reaction time about 80 min. The resulting product has a face-centered cubic crystal structure with characteristic diffraction peaks of AgNPs, showing that the C. AgNPs have a single crystal structure. C. AgNPs were used as photocatalysts for the treatment of MB dye when excited by white light with an irradiation power of 30 W which has a color temperature of 6500 K. These results displayed that in the presence of C. AgNPs, the ability to degrade MB of H_2O_2 and $NaBH_4$ was much improved. MB degradation efficiency is up to 96% in about 60 min illuminated. Our efforts in the synthesis of C. AgNPs using green tea leaf extract have resulted in the production of environmentally friendly, low-cost, and relatively stable particles. This breakthrough offers numerous applications for this material, particularly in the field of biomedicine. However, further improvement is required in achieving better control over the size and shape of AgNPs through the green synthesis method.

Data availability statement

Data included in article/supplementary material/referenced in article.

Additional information

No additional information is available for this paper.

Declaration of competing interest

The authors declare that they have no known competing financial interests or personal relationships that could have appeared to influence the work reported in this paper.

Acknowledgement

The present research was supported by a grant from the Ministry of Education and Training code B2023-TNA-06.

References

[1] S. Sim, N.K. Wong, Nanotechnology and its use in imaging and drug delivery, Biomed Rep 14 (5) (2021), https://doi.org/10.3892/br.2021.1418 submitted for publication.
[2] S. Hamimed, M. Jabberi, A. Chatti, Nanotechnology in drug and gene delivery," Naunyn-Schmiedeberg's Archives of Pharmacology, Jul. 01, Springer Science and Business Media Deutschland GmbH 395 (7) (2022) 769–787, https://doi.org/10.1007/s00210-022-02245-z.
[3] A. Haleem, M. Javaid, R.P. Singh, S. Rab, R. Suman, Applications of nanotechnology in medical field: a brief review, Global Health J. (Jun. 2023), https://doi.org/10.1016/j.glohj.2023.02.008.
[4] A. Aghababai Beni, H. Jabbari, Sep. 01, Nanomaterials for Environmental Applications," *Results in Engineering*, vol. 15, Elsevier B.V., 2022, https://doi.org/10.1016/j.rineng.2022.100467.
[5] E.I. Epelle, P.U. Okoye, S. Roddy, B. Gunes, J.A. Okolie, Advances in the applications of nanomaterials for wastewater treatment, MDPI, Nov. 01, Environments - MDPI 9 (11) (2022), https://doi.org/10.3390/environments9110141.
[6] R. Qadri, M.A. Faiq, Freshwater pollution: effects on aquatic life and human health, in: Fresh Water Pollution Dynamics and Remediation, Springer Singapore, 2020, pp. 15–26, https://doi.org/10.1007/978-981-13-8277-2_2.
[7] B. Chen, et al., In search of key: protecting human health and the ecosystem from water pollution in China, J. Clean. Prod. 228 (Aug. 2019) 101–111, https://doi.org/10.1016/j.jclepro.2019.04.228.
[8] N.Y. Donkadokula, A.K. Kola, I. Naz, D. Saroj, A review on advanced physico-chemical and biological textile dye wastewater treatment techniques, Springer, Rev. Environ. Sci. Biotechnol. 19 (3) (2020) 543–560, https://doi.org/10.1007/s11157-020-09543-z. Sep. 01.
[9] X. Xu, Q. Hou, Y. Xue, Y. Jian, L.P. Wang, Pollution characteristics and fate of microfibers in the wastewater from textile dyeing wastewater treatment plant, Water Sci. Technol. 78 (10) (Dec. 2018) 2046–2054, https://doi.org/10.2166/wst.2018.476.
[10] L. Liu, et al., Treatment of industrial dye wastewater and pharmaceutical residue wastewater by advanced oxidation processes and its combination with nanocatalysts: a review, J. Water Proc. Eng. 42 (2021), https://doi.org/10.1016/j.jwpe.2021.102122. Elsevier Ltd, Aug. 01.
[11] J.K.H. Wong, H.K. Tan, S.Y. Lau, P.S. Yap, M.K. Danquah, Potential and challenges of enzyme incorporated nanotechnology in dye wastewater treatment: a review, J. Environ. Chem. Eng. 7 (4) (2019), https://doi.org/10.1016/j.jece.2019.103261. Elsevier Ltd, Aug. 01.
[12] I. Anastopoulos, A. Hosseini-Bandegharaei, J. Fu, A.C. Mitropoulos, G.Z. Kyzas, Use of nanoparticles for dye adsorption: review, J. Dispersion Sci. Technol. 39 (6) (Jun. 2018) 836–847, https://doi.org/10.1080/01932691.2017.1398661.
[13] Z. Cai, Y. Sun, W. Liu, F. Pan, P. Sun, J. Fu, An overview of nanomaterials applied for removing dyes from wastewater, Environ. Sci. Pollut. Control Ser. 24 (19) (Jul. 2017) 15882–15904, https://doi.org/10.1007/s11356-017-9003-8.
[14] D. Atanasova, D. Staneva, I. Grabchev, Textile with a hydrogel and iron oxide nanoparticles for wastewater treatment after reactive dyeing, J. Appl. Polym. Sci. 138 (10) (Mar. 2021), https://doi.org/10.1002/app.49954.
[15] P. Yu, H. Yu, Q. Sun, B. Ma, Filter paper supported nZVI for continuous treatment of simulated dyeing wastewater, Sci. Rep. 9 (1) (Dec. 2019), https://doi.org/10.1038/s41598-019-47863-5.

[16] M. Chandhru, S.K. Rani, N. Vasimalai, Reductive degradation of toxic six dyes in industrial wastewater using diaminobenzoic acid capped silver nanoparticles, J. Environ. Chem. Eng. 8 (5) (2020), https://doi.org/10.1016/j.jece.2020.104225.
[17] T. Ahmed, et al., Green synthesis of silver nanoparticles transformed synthetic textile dye into less toxic intermediate molecules through LC-MS analysis and treated the actual wastewater, Environ. Res. 191 (Dec. 2020), https://doi.org/10.1016/j.envres.2020.110142.
[18] J. Chen, et al., Konjac glucomannan reduced-stabilized silver nanoparticles for mono-azo and di-azo contained wastewater treatment, Inorg. Chim. Acta. 515 (Jan. 2021), https://doi.org/10.1016/j.ica.2020.120058.
[19] S. Marimuthu, et al., Silver nanoparticles in dye effluent treatment: a review on synthesis, treatment methods, mechanisms, photocatalytic degradation, toxic effects and mitigation of toxicity, J. Photochem. Photobiol., B 205 (Apr) (2020), https://doi.org/10.1016/j.jphotobiol.2020.111823.
[20] J.A. Mazumder, M. Perwez, R. Noori, M. Sardar, Development of sustainable and reusable silver nanoparticle-coated glass for the treatment of contaminated water, Environ. Sci. Pollut. Control Ser. 26 (22) (Aug. 2019) 23070–23081, https://doi.org/10.1007/s11356-019-05647-4.
[21] S. Sarina, E.R. Waclawik, H. Zhu, Photocatalysis on supported gold and silver nanoparticles under ultraviolet and visible light irradiation, Green Chem. 15 (7) (2013) 1814–1833, https://doi.org/10.1039/c3gc40450a. Royal Society of Chemistry.
[22] A.A. Assadi, et al., Synthesis and characterization of TiO2 nanotubes (TiO2-NTs) with Ag silver nanoparticles (Ag-NPs): photocatalytic performance for wastewater treatment under visible light, Materials 15 (4) (Feb. 2022), https://doi.org/10.3390/ma15041463.
[23] A. Jbeli, et al., Chitosan-Ag-TiO2 films: an effective photocatalyst under visible light, Carbohydr. Polym. 199 (Nov. 2018) 31–40, https://doi.org/10.1016/j.carbpol.2018.06.122.
[24] H. Wang, et al., Environmentally benign chitosan as reductant and supporter for synthesis of Ag/AgCl/chitosan composites by one-step and their photocatalytic degradation performance under visible-light irradiation, Front. Mater. Sci. 11 (2) (Jun. 2017) 130–138, https://doi.org/10.1007/s11706-017-0383-y.
[25] A. Kumar, et al., Bio-inspired and biomaterials-based hybrid photocatalysts for environmental detoxification: a review, in: Chemical Engineering Journal, vol. 382, Elsevier B.V., 2020, https://doi.org/10.1016/j.cej.2019.122937. Feb. 15.
[26] S. Sarina, E.R. Waclawik, H. Zhu, Photocatalysis on supported gold and silver nanoparticles under ultraviolet and visible light irradiation, Green Chem. 15 (7) (2013) 1814–1833, https://doi.org/10.1039/c3gc40450a. Royal Society of Chemistry.
[27] S. Marimuthu, et al., Silver nanoparticles in dye effluent treatment: a review on synthesis, treatment methods, mechanisms, photocatalytic degradation, toxic effects and mitigation of toxicity, J. Photochem. Photobiol., B 205 (Apr. 2020), https://doi.org/10.1016/j.jphotobiol.2020.111823.
[28] T. Ahmed, et al., Green synthesis of silver nanoparticles transformed synthetic textile dye into less toxic intermediate molecules through LC-MS analysis and treated the actual wastewater, Environ. Res. 191 (Dec. 2020), https://doi.org/10.1016/j.envres.2020.110142.
[29] I.X. Yin, J. Zhang, I.S. Zhao, M.L. Mei, Q. Li, C.H. Chu, The antibacterial mechanism of silver nanoparticles and its application in dentistry, Dove Medical Press Ltd. Int. J. Nanomed. 15 (2020) 2555–2562, https://doi.org/10.2147/IJN.S246764.
[30] S. Anees Ahmad, et al., Bactericidal activity of silver nanoparticles: a mechanistic review, KeAi Communications Co. Mater. Sci. Energy Technol. 3 (2020) 756–769, https://doi.org/10.1016/j.mset.2020.09.002. Jan. 01
[31] R.P. Illanes Tormena, et al., Evaluation of the antimicrobial activity of silver nanoparticles obtained by microwave-assisted green synthesis usingHandroanthus impetiginosus(Mart. ex DC.) Mattos underbark extract, RSC Adv. 10 (35) (Jun. 2020) 20676–20681, https://doi.org/10.1039/d0ra03240a.
[32] D.T. Hue, N.T.P. Thao, T.K. Khoi, C.V. Ha, Multi-shaped silver meso-particles with tunable morphology for surface enhanced Raman scattering, Opt Commun. 497 (Oct. 2021), https://doi.org/10.1016/j.optcom.2021.127200.
[33] S.A. Razek, A.B. Ayoub, M.A. Swillam, One step fabrication of highly absorptive and surface enhanced Raman scattering (SERS) silver nano-trees on silicon substrate, Sci. Rep. 9 (1) (Dec. 2019), https://doi.org/10.1038/s41598-019-49896-2.
[34] R.X. He, R. Liang, P. Peng, Y. Norman Zhou, Effect of the size of silver nanoparticles on SERS signal enhancement, J. Nanoparticle Res. 19 (8) (Aug. 2017), https://doi.org/10.1007/s11051-017-3953-0.
[35] B. Le Ouay, F. Stellacci, Antibacterial activity of silver nanoparticles: a surface science insight, Elsevier B.V. Nano Today 10 (3) (2015) 339–354, https://doi.org/10.1016/j.nantod.2015.04.002. Jul. 22
[36] S. Tang, J. Zheng, Antibacterial activity of silver nanoparticles: structural effects, 13, in: Advanced Healthcare Materials, vol. 7, Wiley-VCH Verlag, 2018, https://doi.org/10.1002/adhm.201701503. Jul. 11.
[37] F. Hadacek, H. Greger, Testing of antifungal natural products: methodologies, comparability of results and assay choice, Phytochem. Anal. 11 (3) (2000), https://doi.org/10.1002/(SICI)1099-1565(200005/06. May/June.
[38] A.U. Khan, et al., Biosynthesis of silver capped magnesium oxide nanocomposite using Olea cuspidata leaf extract and their photocatalytic, antioxidant and antibacterial activity, Photodiagnosis Photodyn. Ther. 33 (Mar. 2021), https://doi.org/10.1016/j.pdpdt.2020.102153.
[39] K. ur Rehman, et al., Facile synthesis of copper oxide nanoparticles (CuONPs) using green method to promote photocatalytic and biocidal applications, J. Mol. Liq. 360 (Aug. 2022), https://doi.org/10.1016/j.molliq.2022.119453.
[40] P.L. Fernández, M.J. Martin, A.G. González, F. Pablos, HPLC determination of catechins and caffeine in tea. Differentiation of green, black and instant teas, Analyst 125 (3) (2000) 421–425, https://doi.org/10.1039/a909219f.
[41] S.A. Khan, S.B. Khan, L.U. Khan, A. Farooq, K. Akhtar, A.M. Asiri, Fourier transform infrared spectroscopy: fundamentals and application in functional groups and nanomaterials characterization, in: Handbook of Materials Characterization, Springer International Publishing, 2018, pp. 317–344, https://doi.org/10.1007/978-3-319-92955-2_9.
[42] M.A. Huq, Green synthesis of silver nanoparticles using pseudoduganella eburnea MAHUQ-39 and their antimicrobial mechanisms investigation against drug resistant human pathogens, Int. J. Mol. Sci. 21 (4) (Feb. 2020), https://doi.org/10.3390/ijms21041510.
[43] V. Ravichandran, S. Vasanthi, S. Shalini, S.A.A. Shah, M. Tripathy, N. Paliwal, Green synthesis, characterization, antibacterial, antioxidant and photocatalytic activity of Parkia speciosa leaves extract mediated silver nanoparticles, Results Phys. 15 (Dec. 2019), https://doi.org/10.1016/j.rinp.2019.102565.
[44] K. Roy, C.K. Sarkar, C.K. Ghosh, Photocatalytic activity of biogenic silver nanoparticles synthesized using yeast (Saccharomyces cerevisiae) extract, Appl. Nanosci. 5 (8) (Nov. 2015) 953–959, https://doi.org/10.1007/s13204-014-0392-4.
[45] I.X. Yin, J. Zhang, I.S. Zhao, M.L. Mei, Q. Li, C.H. Chu, The antibacterial mechanism of silver nanoparticles and its application in dentistry, Int. J. Nanomed. 15 (2020) 2555–2562, https://doi.org/10.2147/IJN.S246764. Dove Medical Press Ltd.
[46] E. Urnukhsaikhan, B.E. Bold, A. Gunbileg, N. Sukhbaatar, T. Mishig-Ochir, Antibacterial activity and characteristics of silver nanoparticles biosynthesized from Carduus crispus, Sci. Rep. 11 (1) (Dec. 2021), https://doi.org/10.1038/s41598-021-00520-2.